SPE 164489

Modeling and Analysis of Salt Cavern Natural Gas Storage

P. Barajas and F. Civan, SPE, the University of Oklahoma

This paper was prepared for presentation at the SPE Production and Operations Symposium held in Oklahoma City, Oklahoma, USA, 23−26 March 2013.

Abstract

A rigorous modeling approach is developed for effective management and inventory analysis of natural gas storage in underground salt caverns by considering the interactions of storage gas with surface facilities through wells and surrounding salt formation. Computational fluid dynamics and heat transfer modeling approaches are implemented to simulate the strongly-coupled fluid mechanics and heat transfer problems involving the cavern gas storage. Effective numerical methods and algorithms implemented in this work successfully generate the wellbore temperature and pressure distributions, gas cavern temperature, pressure, and velocity distributions, and temperature and pressure distributions of the gas leaking into the surrounding naturally-fractured salt formation. Practical applications are performed concerning typical gas injection, storage, and production scenarios and inventory analyses for regular and irregular shaped caverns. Reversible and irreversible losses of natural gas into surrounding salt formation through natural defects such as natural fractures and defects resulting from deformation, ballooning, and aging effects are taken into account. Maximum amounts of gas that can be stored up to the pressure safety limit of caverns are shown to vary with the cavern shapes. Thus, the cavern gas inventory analysis is not only dependent on temperature, pressure, and total volume of the cavern but also the cavern shape. Accurate prediction of the natural gas storage performance and inventories based on the present comprehensive simulation approach can be instrumental in effective management and balancing of the natural gas supply and demand.

Introduction

Gas storage caverns are typically developed through drilling of a wellbore to reach the salt formation and subsequently by injecting and circulating hot water to dissolve and remove the salt and create a cavity intended for gas storage by a process known as solution mining. Gas storage cavern facilities consist of three subsystems, the wellbore that connects surface facilities with the cavern, the cavern, and the surrounding salt formation that encloses the cavern (Figure 3). Accurate prediction of cavern gas pressure is important for avoiding improper gas storage operation parameters and thus fracturing and failure of the salt formation and hence the cavern roof collapse which can lead to catastrophic incidents where the stored gas migrates towards the ground surface and causes injuries to field personnel and damage to surface facilities and nearby population. On the other hand, loss of volume due to creep closure can occur when the cavern gas pressure drops below the minimum allowable cavern pressure. Effective management and inventory analyses of underground natural gas storage are generally accomplished by modeling and simulation of the gas conditions in the storage media (Civan 2004; Liu and Civan 2005).

The complete storage process initiates with gas injection followed by gas storage (during surplus periods) and finalizes with gas production or withdrawal (over-demand seasons). The increasing popularity of salt caverns is attributed to their flexibility to quickly switch from gas injection to gas production. The void space of the cavern does not cause pressure loss from flow restrictions in contrast to depleted reservoirs or aquifers. Ideally stored gas cannot leak into the surrounding naturally fractured salt formation because of its approximately negligible porosity and permeability. Typical gas caverns in salt formations are located at depths between 1000 to 2000 meters with internal physical volumes ranging between 1.0 to $5.0x10^5$ m^3 with maximum operating pressures of 150 to 250 Bar and maximum gas inventories in capacity of 15 to $150x10^6$ m^3 of natural gas (Hagoort 1994; Tek 1996). Thickness of salt formations can vary typically from a few meters in salt beds to thousands of meters in salt domes.

Salt-cavern type underground storage is the fastest growing gas storage option. In fact, 37 salt cavern fields were present in the US in the year 2010. In the last 5 years the US has almost doubled salt cavern storage capacity (EIA database). In Europe there were 46 salt cavern fields by 2007. Natural gas supply from remote regions is shifting pipelines to LNG chain.

LNG tankers require unloading the LNG within only a few hours upon arrival at receiving terminals. The LNG is then converted into a gaseous form using proper processing equipment and is immediately injected into salt caverns at cavern pressure. New gas caverns with improved designs are required considering the extremely fast unloading times of a tanker containing sufficient amount of gas to fill the full working gas volume capacity of a typical gas cavern (Gillhaus 2007).

The present modeling approach is carried out for prediction of the cavern gas operation conditions (pressures and temperatures), and quantification of the volume of gas present in the cavern at any time to monitor assets and losses through the inventory analysis. Inventory is the volume of gas present in the cavern at any point in time and is composed from the working- and cushion-gas portions of the stored gas. This volume of gas depends on the prevailing pressure and temperature, and type and size of the cavern (Tek 1996). We develop a modeling approach for accurate natural gas storage and inventory analysis and management in underground salt caverns. We consider the interactions of the storage gas with surface facilities through the wells and surrounding salt formation. We apply a computational fluid dynamics and heat transfer (CFD) approach to simulate the coupled problems of fluid mechanics and heat transfer involving the cavern storage by means of effective numerical methods and algorithms to describe the gas storage problem properly in a practical and precise manner. We first demonstrate the model capabilities by simulating gas storage for prescribed cavern shapes. The modeling approach generates wellbore temperature and pressure distributions, gas cavern temperature, pressure, and velocity distributions, and temperature and pressure distributions of the gas which leaked-off into the surrounding naturally-fractured salt formation. We then demonstrate the practical applications of this simulation tool by predicting typical gas injection, storage, and production behaviors and carry out an inventory analysis for regular and irregular cavern shapes for comparison purposes. Additionally, we determine the reversible and irreversible losses of natural gas into the surrounding salt formation because of defects such as natural fractures and faults resulting from deformation, ballooning, and aging effects.

The accuracy of this simulator is established by comparing the results of the present simulations with those obtained under various simplified conditions in previous studies. Typical scenarios of gas storage simulations are presented here for realistic cases of practical importance. The results indicate that the gas pressure increases in the cavern significantly during the injection phase, slightly decreases during storage essentially because of gas leak-off and cooling effects, and decreases during production. Cavern shapes such as inverted cone and sphere resulted in lower operating gas pressures than cylindrical shape, and therefore more gas can be stored safely before reaching the maximum allowable cavern pressure. Our investigation of the effect of cavern shape on gas storage modeling and inventory analysis demonstrated that not only temperature, pressure, and total volume affect cavern gas inventories as stated by previous authors but also cavern shape (Hagoort 1994; Tek 1996). Our comprehensive simulator can provide gas storage companies an ability to accurately predict the natural gas storage performance and cavern gas inventories which are important for effective management of the natural gas supply-demand market.

Critical Review of Modeling Approaches

The publicly available reports on salt cavern gas storage are primarily concerned with geology, rock mechanics, and solution-mining for salt caverns (Harmut et al. 2006; Hilbert and Saraf 2008; DeVries et al. 1994; Han et al. 1994; Berest 2003). A complete set of equations for underground gas storage can be found in the literature (Tek 1996). However, only few studies have dealt with the simulation approaches focused on the gas injection, storage, and production behavior and the gas inventory analysis (Hagoort 1994; Steinberger et al. 2002; Iloeje 2006).

Hagoort (1994) presented a basic mathematical model to estimate the injection and production performances of gas storage caverns in salt formations. This model neglects the heat exchange of the wellbore gas with the surroundings and considers only the caverns of cylindrical shape. The pressure and temperature in the cavern are assumed spatially uniform at all times. This model also assumes that the salt formation is a perfect barrier for the gas leakage through the salt formation.

Steinberger et al. (2002) developed a model that considered the effect of hydrocarbon thermodynamics, phase separation behavior, and heat and mass exchanges along cavern walls during gas loading, storage, and unloading. The temperature and pressure are assumed uniformly distributed throughout the cavern.

Iloeje (2006) presented a modeling approach that included more realistic factors than the previous studies. However, the cavern shape was approximated as a cylinder and the properties of the gas throughout the cavern were assumed uniform. Nevertheless, Iloeje (2006) included the effect of interactions of the cavern gas and the surrounding salt formation.

Figure 1 shows the physical model considered in the best of the above-mentioned previously available models. All the assumptions made in the previous studies required extensive modeling and programming. In this paper, we evaluate the considerations of the previous models for different cavern shapes. Although frequently a regular shape, such as cylindrical, spherical, or inverted cone shapes (API Recommended Practice 1114) is attempted in the solution mining process, the resulting salt cavern shape is usually obtained as an irregular shape. The shape and size of the resulting cavern are confirmed with sonar measurements or any other appropriate logging tools. The vertical pressure gradient can be significant for considerably large-size caverns and hence the uniformly distributed average pressure assumption of the previous modeling attempts may not be appropriate. Further, the previous models are not designed for realistic irregular cavern shapes of practical interest.

With the objective of avoiding extensive programming, we resort to a computational fluid dynamics (CFD) modeling approach for simulation and analysis of the salt cavern natural gas storage in various shape salt caverns. The simulation models for three subsystems, namely the wellbore, cavern, and salt formation, involved in the storage process are presented.

The transient-state wellbore mass, momentum, and energy balances are considered including the heat exchange with the surrounding formation. The cavern gas undergoes transient-state pressure and temperature spatial distributions. Cavern shape can be taken as one of the API prescribed shapes, namely cylindrical, spherical, and inverted cone (API Recommended Practice 1114) as well as the actual measured irregular shapes resulting from the solution mining process. Hydrocarbon condensation and brine presence are assumed negligible. The interactions between the cavern gas and the surrounding salt formation include the heat and mass exchange across the cavity wall. The salt formation undergoes a transient pressure and temperature spatial distribution. **Figure 2** shows a similar trend between the pressure results of a simulation made to compare and validate our modeling approach under the same operating conditions of the simulation made by Iloeje (2006). However, our results are expected to be better because of our improved numerical computation.

Physical Model

Figure 3 is a schematic of the physical model considered in this study for simulation of the three subsystems involved in gas storage cavern operations. This is a more realistic physical model than the one shown in Figure 1. The considerations of the mass, momentum, and energy balance in the wellbore are a transient-state process and the heat exchange with the surroundings is considered. The large gas cavern includes the transient pressure and temperature spatial distributions. The best of the previously available models considers less than 50% of the factors involved in a real gas storage process. In addition, the best previously available model is only applicable for a cylindrical shape cavern whereas the shapes resulting from solution mining are usually different from cylinder.

For the first part of the present modeling applications, a geometrical system that resembles the physical model of the three cavern subsystems is constructed as illustrated in Figure 3. The physical dimensions of the cavern and the salt formation were defined considering the API recommended practice for the minimum distance between two neighboring caverns (API Recommended Practice 1114). The suitable numerical gridding distribution is assigned for the cavern geometry system using GAMBIT software which can create both structured and unstructured grids for orthogonal and non-orthogonal geometries that could not be considered in the previous modeling approaches. The boundary conditions are defined in GAMBIT. The grid system is exported into ANSYS FLUENT where the boundary and initial conditions are provided as input. The numerical solution method is selected and the initial conditions are set to initialize the simulation. ANSYS FLUENT solves the governing equations of mass, momentum, and energy applied over each control volume of the cavern system for each time step using a finite-volume difference method. The solution is finalized when the specified convergence criteria is reached after each time step. As a further revision of the accuracy of results, a grid sensitivity analysis with different grid sizes is carried out to ensure that the simulation results are independent of grid sizes. Ultimately, the numerical and graphical results of the three subsystems are properly processed to describe gas storage dynamics during injection, storage, and production, and to perform a cavern inventory analysis. The computational time of the simulations greatly depends on the geometry of the cavern, type of gridding system, and required accuracy of the simulation as well as the computer hardware used. For instance, a cylindrical cavern model composed of an orthogonal (structured) gridding system with 324 control volumes has an approximate ratio of real time to computational time of 8 hours to 1 hour, whereas a cavern system with a shape of an inverted cone using an unstructured gridding system with 5576 control volumes has an approximate ratio of 2 hours of real time to 1 hour of computational time.

Coupling of Thermo-hydraulics of Wellbore, Cavern, and Salt Formation

Modeling the injection, storage, and production of natural gas in underground salt caverns requires the energy, momentum, and mass conservation equations be solved simultaneously. Additionally, modeling of naturally fractured salt formation represented as a porous media of near-zero porosity requires specific additional source terms in the momentum and energy equations. ANSYS FLUENT software solves the equations of density of real gas, and mass, momentum, and energy conservations for each control volume of fluid of the wellbore, cavern, and salt formation. The naturally fractured salt formation is represented as porous media of permeability near-zero. Its permeability is essentially due to the natural fractures formed by stress deformation of brittle salt formation. The control volumes in the porous media are solved with the momentum equation with a porous media term and also a specific porous media energy equation is used by fluent. The governing equations are described as follows (ANSYS FLUENT User Guide 2009). Density of gas, continuity (conservation of mass), and conservation of momentum are given, respectively by:

$$\rho = \frac{PMW}{zRT} \tag{1}$$

$$\frac{\partial \rho}{\partial t} + \frac{\partial}{\partial x}(\rho v_x) + \frac{\rho}{\partial r}(\rho v_r) + \frac{\rho v_r}{r} - 0 \tag{2}$$

$$\frac{\partial \rho}{\partial t}(\rho \vec{v}) + \nabla \cdot (\rho \vec{v}\vec{v}) = -\nabla p + \nabla \cdot (\bar{\bar{\tau}}) + \rho \vec{g} + \vec{F} \tag{3}$$

ρg is the gravitational body force in the vertical direction (represented in the equation as x direction), v is the velocity, $\bar{\bar{\tau}}$ is the stress tensor which is a function of the dynamic viscosity and the velocity and P is the static pressure.

The mass flow from the cavern to the porous media is described with a source term $\vec{F}$ used to represent the salt formation. The source term is composed of two parts: a viscous loss (first term on the right side of equation 4 and 5) and an inertial loss term (second term on the right side of equation 4 and 5). The leak-off flow is assumed laminar; therefore the inertial term is negligible. The resulting equation is known as the Darcy's law in porous media. Salt formation terms in the axial and radial directions are given respectively by:

$$F_x = -\left(\frac{\mu}{\alpha_x} u_x + C_2 \frac{1}{2} \rho u_x^2\right) \quad (4)$$

$$F_r = -\left(\frac{\mu}{\alpha_r} u_r + C_2 \frac{1}{2} \rho u_r^2\right) \quad (5)$$

Gas flow in this simulation also involves heat transfer thus requires additional equations for energy conservation. Equation 6 shows the energy equation for the gas flowing in wellbore and cavern:

$$\rho c_p \frac{\partial T}{\partial t} + \rho c_p \left[u \frac{\partial T}{\partial x} + v \frac{\partial T}{\partial r}\right] = k\left[\frac{\partial}{\partial x}\left(\frac{\partial T}{\partial x} - uT\right) + \frac{1}{r}\frac{\partial}{\partial r}\left(r\left(\frac{\partial T}{\partial r} - vT\right)\right)\right] + \frac{h_v(T_s - T)}{\varphi} \quad (6)$$

Here k is the thermal conductivity of the gas, T is the temperature and φ is the porosity of the porous medium where the gas is flowing through.

The heat transfer in the porous region of the naturally fractured salt formation is modeled by introducing a thermal inertia of solid region on the medium (in the transient term) to the salt formation energy equation and by an effective thermal conductivity in the conductive flux (ANSYS FLUENT User Guide 2009).

$$\frac{\partial T_s}{\partial t} = \frac{k_s}{(1-\varphi)\rho_s c_{p_s}} = \left[\frac{\partial}{\partial x}\left(\frac{\partial T_s}{\partial x}\right) + \frac{1}{r}\frac{\partial}{\partial r}\left(r\frac{\partial T_s}{\partial r}\right)\right] - \frac{h_v(T_s - T)}{(1-\varphi)\rho_s c_{p_s}} \quad (7)$$

Subscript s refers to the solid naturally fractured salt formation. The local thermal non-equilibrium between the cavern gas and the salt formation was modeled by solving two separate energy equations and coupling them through a volumetric heat transfer coefficient. The interfacial volumetric convective heat transfer is used to couple the two equations. The heat transfer coefficient h_v is calculated from the Nusselt number correlation (ANSYS FLUENT User Guide 2009).

$$h_v = \frac{Nu_s k}{d_p^2} \quad (8)$$

Model Considerations and Conditions of Simulations

Boundary conditions specify the flow and thermal variables on the boundaries of the gas cavern model. They are therefore a critical component of the simulations with ANSYS FLUENT which should be specified properly. The boundary conditions assigned in GAMBIT during the development of the physical model are illustrated in **Figure 4**. **Table 1** summarizes the boundary conditions used in simulations to demonstrate the capabilities of the present modeling approach. The mass flow rate at the wellhead was used as 38 kg/s equivalent to a volumetric flow rate of 175000 scm/hr with an initial pressure of 11000 kPa (Tek 1996). Wall boundary conditions are used to set the thermal parameters at the wall of the salt formation for heat transfer calculations. This type of boundary condition was set at the wall of the wellbore and the outer physical boundary of the salt formation in the radial and axial direction. The wellhead temperature was set at 312 K and the geothermal gradient for the wall temperature was taken as 0.02 ^{o}C/m (Tek 1996). Symmetry boundary condition was used by taking advantage of the symmetry of the physical geometry of interest and the flow/thermal solution (ANSYS FLUENT User Guide 2009). All the caverns modeled had a corresponding equivalent volume of 565000 m^3 (Iloeje 2006).The wellbore length was taken as 1500 m and the wellbore diameter was taken as 0.22 m and was assumed to be equal to the depth from the wellhead to the top of the cavern (Iloeje 2006). The wellhead pressure and temperature were chosen based on typical gas injection temperatures and pressures given by storage companies (Tek 1996). Cavern volumes typically range between 500,000 and 800,000 m^3. The apparent permeability representing the naturally occurring fractures of the salt formation is typically small, and values range from 10^{-18} to 10^{-22} m^2 (Iloeje 2006).

Simulation Results

The data obtained from the simulations are analyzed and graphed properly for the injection-storage-production cycle of a prescribed shape cavern (inverted cone shape) for purposes of demonstration of capabilities of our modeling approach. The effect of the cavern shape in gas cavern pressure and temperature is demonstrated by simulating cylindrical and spherical caverns. In addition, we introduce an irregular-shape cavern gas modeling and compare the pressure and temperature values to the corresponding regular shape of equal volume. The pressure and temperature along the wellbore increase from the wellhead as the gas travels along the wellbore closer to the salt cavity. The pressure differential between the wellhead and the top of the cavern is around 1200 kPa. **Figure 5** describes the temperate and pressure profiles at different times of gas injection. Previous models considered uniform pressure throughout the cavern at any point in time. **Figure 6** shows that cavern gas pressure varies with locations in the cavern. The highest gas pressure is found at the bottom of the cavern. The radial gas pressure gradient is negligible. This information is important to avoid exceeding the maximum allowable working pressure of the formation. **Figure 7** shows the temperature gas distribution at different instants, indicating a slightly warmer gas at the bottom of the cavern. The temperature distribution inside the cavern is almost uniform. The graph on the right shows the cooling effects of gas production phase where gas has been removed from the cavern system.

Figure 8 shows the average cavern pressures and temperatures for prescribed regular shapes. In general, for all the shapes, the cavern pressure increases during injection period and decreases during production period. This is attributed to the changes in mass of the gas in the cavern. The mass of gas in the cavern increases for injection and the mass of gas in the cavern decreases as gas is being removed from the cavern during the production period. The cavern pressure slightly drops immediately after the wellbore is shut in at the beginning of the storage period and maintains about the same pressure while the gas is being stored over a period of time. The pressure drops during production. The results for average pressure and temperature are comparable to those presented in previous studies (Iloeje 2006; Steinberger et al. 2002).

Figure 9 presents gas cavern velocity distribution during injection. These contours describe the gas recirculation motion inside the cavern. The gas velocity ranges from 0 at the cavern wall boundaries to 15 m/s at certain locations of the cavern. This information can be instrumental for practicing engineers concerned with the erosion effects in the solution-mined cavern. **Figure 10** presents the pressure distribution of gas in the naturally-fractured salt formation at time of 480 minutes at the end of the of the injection period and at time 1320 minutes which correspond to 360 minutes after the start of gas production. The pressure of the far formation at the instant of injection is lower than the pressure in the vicinity of the cavern. In contrast, the pressure of the far of the formation at the instant of production is higher than the pressure in the vicinities of the cavern. The change in formation pressure does not vary significantly when switching from gas injection to production. **Figure 11** presents temperature distribution at time of 480 minutes at the end of the of the injection period and at time 1320 minutes which correspond to 360 minutes after the start of gas production. The effect of gas cooling at the instant of production on the temperature of the far in formation is higher than the pressure in the vicinity of the cavern.

Gas leakage into the formation occurs because of the pressure differential existing between the salt formation and cavern gas pressures (Steinberger et al. 2002). Gas leaks out of the formation when the cavern pressure exceeds the salt formation pressure. Conversely, gas leaks back into the cavern when cavern pressure is lower than the salt formation pressure. However, the salt formation pressure does not vary significantly during the mass exchange process with the cavern. This can be attributed to the fact that the amount of gas leakage is small because the apparent permeability of the salt formation is very low in the orders of 10^{-18} m^2. **Figure 12** shows the mass exchange between the cavern and the salt formation. Positive values indicate gas leak-off while negative values represent gas leak-in.

Gas Inventory

The sum of the working and cushion gases that are present in the storage cavern at any point in time are referred to as the gas inventory. This volume of gas is dependent on the pressure, cavern type, and size of the cavern (Iloeje 2006). For the gas inventory calculations, ANSYS FLUENT also solves for temperature, pressure, and compressibility factor at each control volume and averages them over the total volume of the cavern. After suitable manipulations, the gas cavern volume at standard conditions is determined at different times of the storage process. The equation of inventory is derived as follows:

$$V[scm] = \frac{PVT_{sc}z_{sc}}{TzR_{sc}} = \frac{P[Bar] \cdot V[m^3] \cdot 298 \cdot 1.0}{T \cdot z \cdot 1.0} \quad (9)$$

Gas inventories are presented by hysteresis plots, in which the average bottomhole pseudo-pressure (P/z) is plotted against inventory in the units of standard volume. **Figure 13** shows that the hysteresis plots of the injection and production curves are very close because of low mass losses for the 1440-minutes cavern operation. **Figure 14** shows the average cavern pressure and temperature for three prescribed cavern shapes. In general, for all the shapes, the cavern pressure increases during injection period and decreases during production period. This is attributed to the changes in mass of the gas in the cavern. The mass of gas in the cavern increases for injection and decreases as gas is being removed from the cavern during the production period. The cavern pressure drops slightly immediately after the wellbore is shut in at the beginning of the storage period and maintains about a constant pressure while the gas is being stored. The pressure drops during production. The

results for average pressure and temperature in the cylindrical cavern are comparable to those presented in previous studies (Iloeje 2006; Steinberger et al., 2002). The inverted conical cavern shows that the pressure exerted against the cavern walls is more than that of the cylindrical and spherical caverns for the same gas injection rate.

Our modeling approach can also help the practicing engineers perform gas injection, storage, and production simulations and inventory analysis for irregular-shape caverns for which the actual shape and size can be determined with sonar or other appropriate logging tools. **Figure 15** shows the regular and irregular shape caverns, for example. The irregular shaped cavern resembles the resulting cavern development attempt**. Figure 16** presents the cavern pressure distribution at different times during gas injection and production for an irregular cavern shape configuration. The highest pressure is found at the bottom of the cavern. The pressure in the cavern increases with the time of injection. Irregular shape caverns follow the same trend as the regular shapes. **Figure 17** shows the average cavern pressure and temperature for the irregular cavern geometry. The standard cavern presented above is used as a reference on this graph. In general, the cavern pressure increases during injection period and decreases during production period. Ensuring that regular and irregular cavern shapes do not differ significantly in the gas storage performance can result in less time consuming simulations because the regular shape simulations would be faster if they can sufficiently approximate the real cavern shapes.

Discussion, Conclusions, and Recommendations

The three subsystems involved in gas cavern storage have been successfully modeled using computational fluid dynamics (CFD) software. The present approach can perform realistic cavern modeling by considering transient and spatial distributions of gas conditions in the wellbore, cavern, and salt formation for any prescribed cavern shape. The disadvantages of this modeling approach are the associated software license cost and that ANSYS FLUENT does not solve directly for the structural analysis of salt formation.

The present modeling approach has successfully modeled the following salt cavern gas issues: (1) Wellbore temperature and pressure distribution. (2) Gas cavern temperature, pressure, and velocity distributions and (3) Salt formation temperature and pressure distributions. The gas pressure and temperature increase in the cavern during the injection phase, remain approximately constant during storage, and decrease during production. This trend also holds for inventories. Spherical caverns resulted in lower operating gas pressures than other shapes. Thus, more gas can be stored in sphere caverns than others before reaching the maximum allowable safety limit of the cavern pressure. This is advantageous because it reduces the risk of salt formation fracturing and other damage, and therefore avoids dangerous gas migration issues. Also the cavern shape in addition to temperature, pressure, and total volume affects the cavern gas inventories.

With the current modeling approach practicing engineers can perform gas injection, storage, and production simulations and inventory analyses for real irregular-shape caverns. The present simulation efforts should be coupled to Finite Element Analysis (FEA) software to perform a rigorous structural analysis of the salt formation.

The present convenient and effective modeling approach enables the gas storage engineers to focus on particular problems of salt cavern storage instead of the tedious software development issues.

Nomenclature

A	Total surface area of the cavern, m^2
c	heat capacity, kJ/kg·K
d	Diameter of wellbore, m
D_1	Diameter of cavern top, m
D_2	Diameter of cavern base, m
f	Friction factor
g	Acceleration due to gravity, m/s^2
h	Cavern height, m
h_v	Volumetric convective heat transfer coefficient, $W/m^2 \cdot K$
k	Heat conductivity of the salt, W/m·K
L	Length of the wellbore, m
m	Mass of gas, kg
$\dot{m}$	Mass flow of gas, kg/s
MW	Molecular weight of gas, kg/kmol
P	Gas pressure (absolute), kPa
P_{form}	Formation pressure (absolute), kPa
$\dot{Q}$	Heat flux, W/s
r	Radial direction, m
R	Universal gas constant, W/s
t	Time, s
T	Gas temperature (absolute), K
T_{form}	Formation temperature (absolute), K

$\vec{v}$	Velocity vector, m/x
V	Velocity magnitude, m/s
x	Vertical direction, m
z	Real gas deviation factor, dimensionless
α	Porous media permeability, m^2
φ	Porous media porosity, dimensionless
γ	Gas specific gravity, fraction
μ	Gas viscosity, cp
ρ	Gas density, kg/m^3
∇	Gradient

References

Ansys Fluent. Version 12.1. 2009. Fluent Inc.

API RP 1114, Recommended Practice for the Design of Solution-Mined Underground Storage Facilities, first edition. 1994. Washington, DC: API.

Bary, A., Schlumberger. 2002. "Storing Natural Gas Underground" Oilfield Review, Vol 14, issue 2, June 2002. http://www.slb.com/resources/publications/industry_articles/oilfield_review/2002/or2002sum01_storing_naturalgas.aspx (downloaded 30 October 2011).

Berest, P. and Brouard, B. 2003. "Safety of Salt Caverns Used for Underground Storage "Oil and Gas Science and Technology, Rev IFP Vol 58, p 361-384.

Civan, F. 2004. “Natural Gas Transportation and Storage,” Encyclopedia of Energy, Cleveland, C. (ed.), Elsevier Inc., Vol. 4, pp. 273-282.

DeVries, K., Callahan, G. and Mellegard, K. 2005. “Numerical Simulations of Natural Gas Storage”. ARMA 05-734. The 40th U.S. Symposium on Rock Mechanics, Anchorage, Alaska, June 25-29, 2005.

Energy Information Administration. 2010. Public database, http:// www.eia.doe.gov/ (accessed 2 November 2012).

Gambit, version 2.1. 2000. Fluent Inc.

Gillhaus, A., KBB. 2007. “Natural Gas Storage in Salt Caverns - Present Status, Developments and Future Trends in Europe”. Solution Mining Research Institute Spring 2007 Conference. 29 April - 2 May, 2007 Basel, Switzerland.

Guangjie, Y., Shen, R., Tian, Z, et al. 2006. “Review of Underground Gas Storage in the Bedded Salt Deposit in China”, SPE Gas Technology Symposium, May 2006.

Han, G., Bruno, M. and Young, J. 1994. “Gas Storage Operations in Single-Bedded Salt Caverns: Stability Analyses”, Published in SPE Reservoir Engineering, November 1994, p. 278-282.

Harmut V., Lorenzo M. 2006. “Controlled Cavern Leaching in Bedded Salt without Blanket in Timpa del Salto”, Solution Mining Research Institute Spring 2006 Conference. 30 April- 3 May, 2006 Brussels, Belgium.

Hagoort, J. “Simulation of Production and Injection Performance of Gas Storage Caverns in Salt Formations”, Paper SPE 26654, SPE Reservoir Engineering, November 1994, p. 278-282.

Hilbert, L., Saraf, V. 2008 “Salt Mechanics and Casing Deformation in Solution-Mined Gas Storage Operation. ARMA 08-383. The 42nd U.S. Symposium on Rock Mechanics, San Francisco, California, June 29 - July 2, 2008.

Iloeje, A. 2006 “Dynamic Mathematical Model for Underground Gas Storage in Salt Cavern,” MS Thesis, University of Oklahoma, Norman, Oklahoma (May 2006).

Liu, N. and Civan, F. 2005. “Underground Gas Storage Inventory Analysis by a Noniterative Method,” Journal of Energy Resources Technology, Vol. 127, No.2, pp. 163-165, June 2005.

Steinberger, A., Civan, F., and Hughes, R.G. 2002. “Phenomenological Inventory Analysis of Underground Gas Storage in Salt Caverns,” Paper SPE 77346, SPE Annual Technical Conference and Exhibition, San Antonio, Texas, 29 September–2 October 2002, and SPE/ISRM Rock Mechanics Conference, Irving, Texas, 20-23 October 2002.

Tek, M. 1996. “Natural Gas Underground Storage: Inventory and Deliverability”, first edition, Tulsa, Oklahoma: Penn Well Publishing Co.

Table 1: Input data for cavern gas storage simulations

Input Information	
Grid density (Model accuracy)	High
Gas composition	Methane
Cavern shape	Cylindrical, Spherical, Inverted Cone
Injection Time	480 minutes
Storage Time	480 minutes
Production Time	480 minutes
Cavern Volume	565000 m^3
Injection/Production rate	38 kg/s (175000 scm/hr)
Wellbore length	1500 m
Wellbore diameter	0.22 m
Initial wellhead pressure	110 Bar
Initial wellhead temperature	288 K
Geothermal Gradient	0.02 K/m
Salt formation permeability	10^{-18} m^2
Salt formation external boundary location (radial and axial)	30 m (above and below cavern), 2 times maximum cavern radius
Salt formation porosity	1%
Salt formation density	2200 kg/m^3
Salt formation specific heat	840 J/kg-K
Salt formation thermal conductivity	5.24 W/m-K

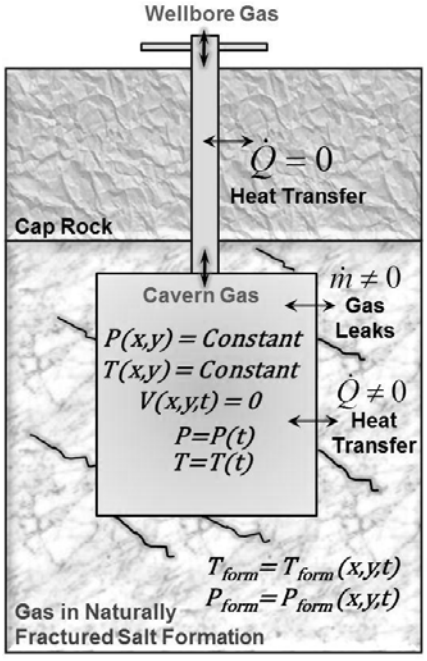

Figure 1: Previous physical model for simulation of gas storage cavern operation

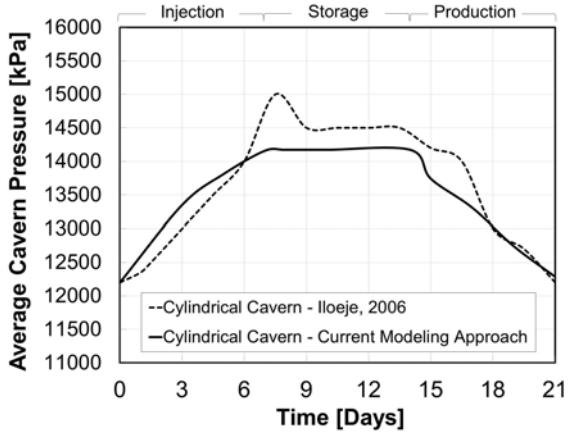

Figure 2: Comparison of the cavern gas pressures predicted by Iloeje (2006) and the present modeling approach

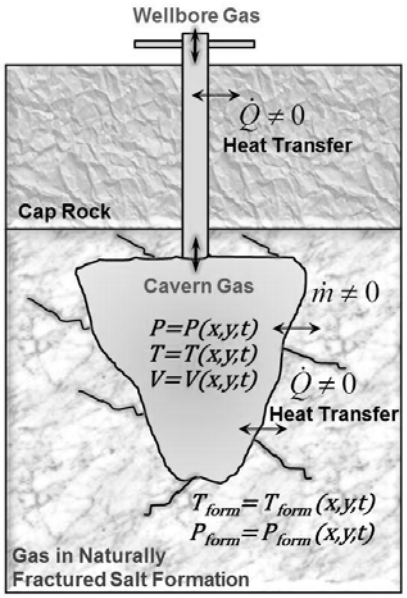

Figure 3: Present physical model for simulation of gas storage cavern operation

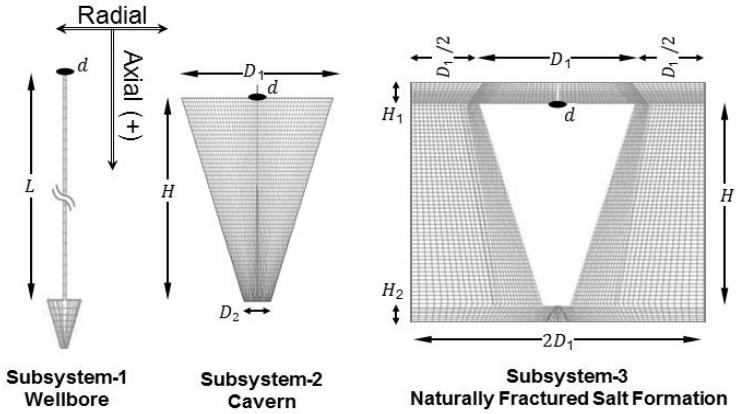

Figure 4: Three subsystems in cavern gas storage operation

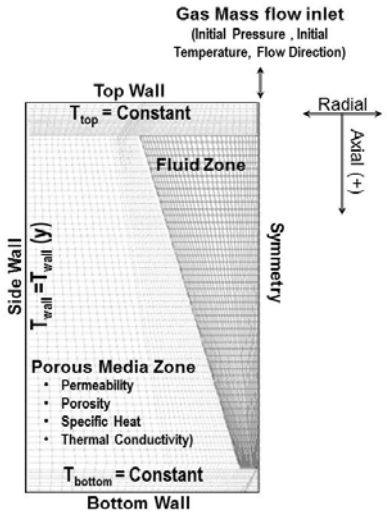

Figure 5: Boundary conditions of the present cavern gas storage model

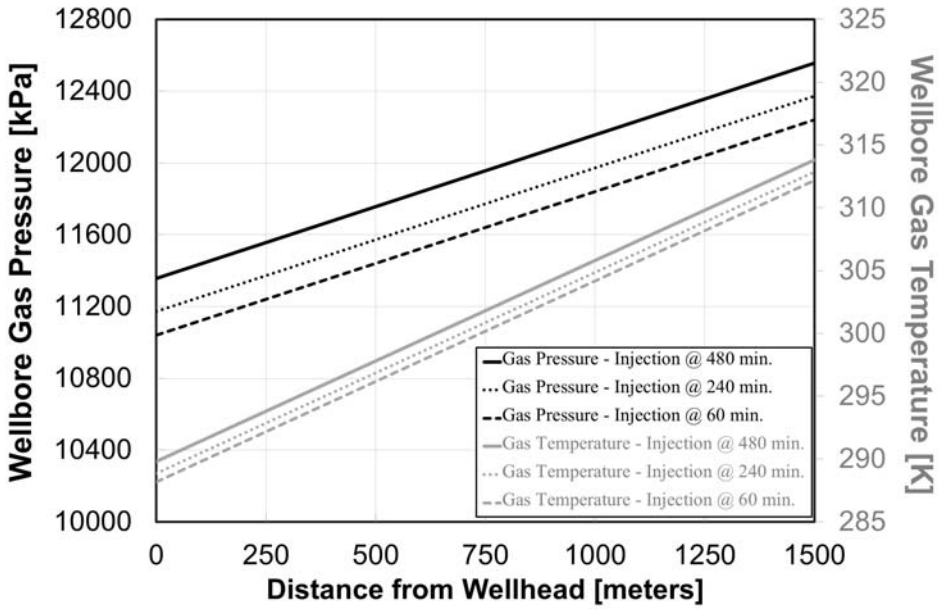

Figure 5: Wellbore flowing pressure and temperature at different gas injection times

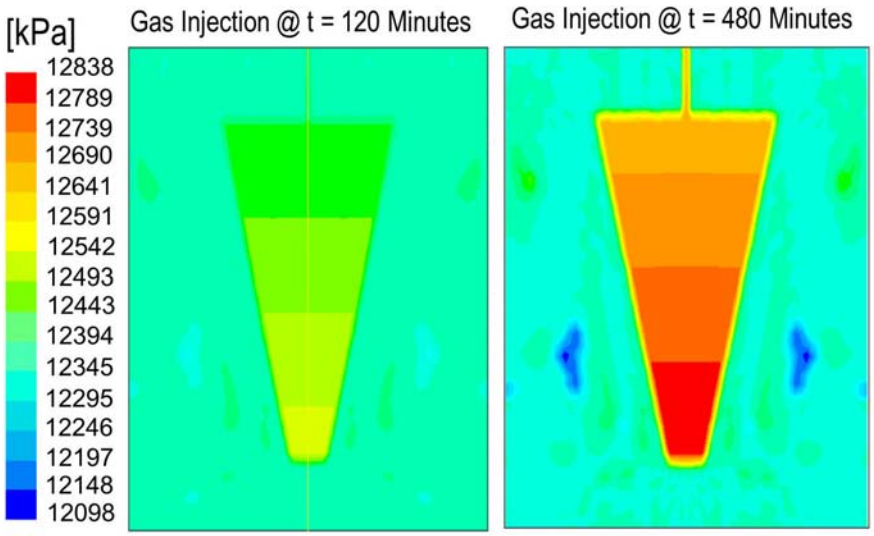

Figure 6: Cavern gas pressure distribution

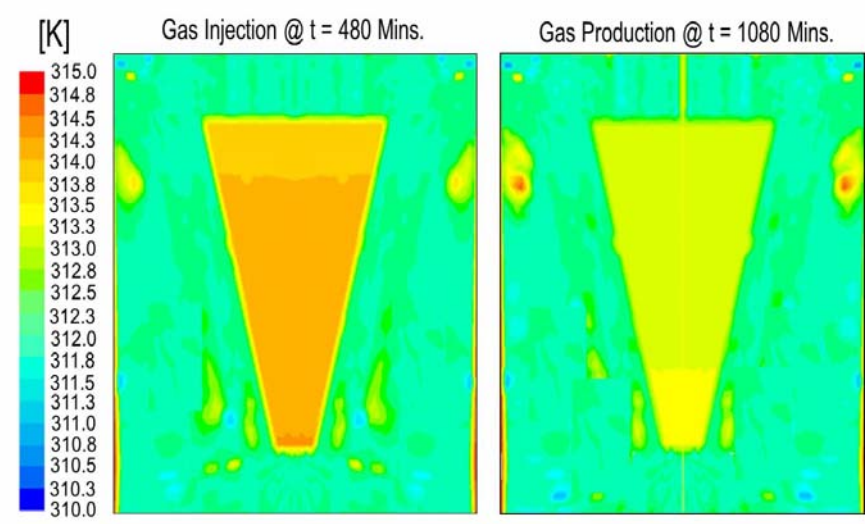

Figure 7: Cavern gas temperature contours

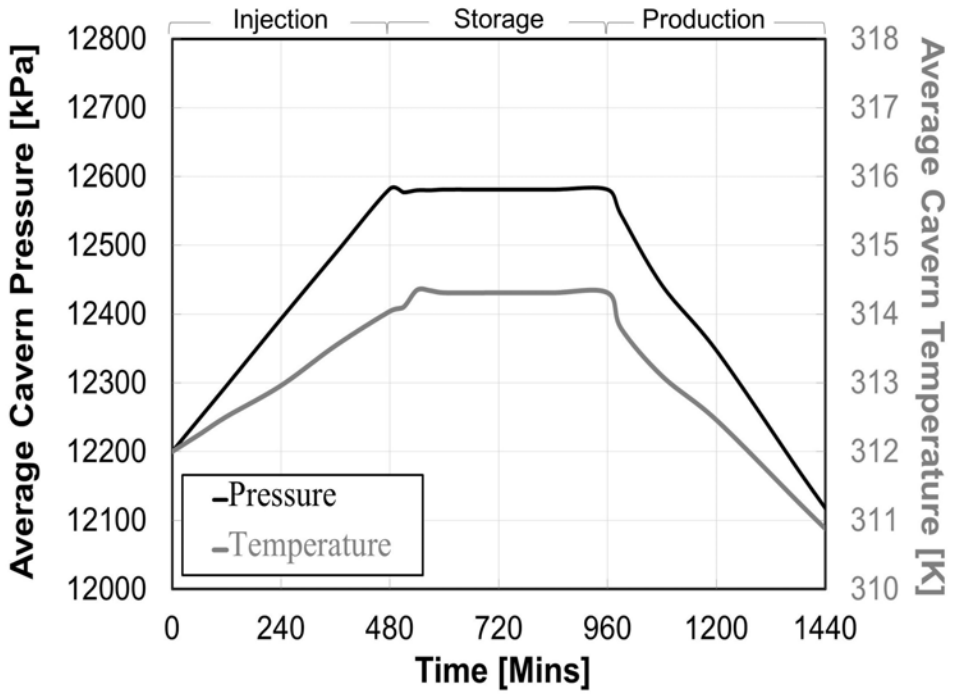

Figure 8: Average cavern gas pressure and temperature during injection, storage and production

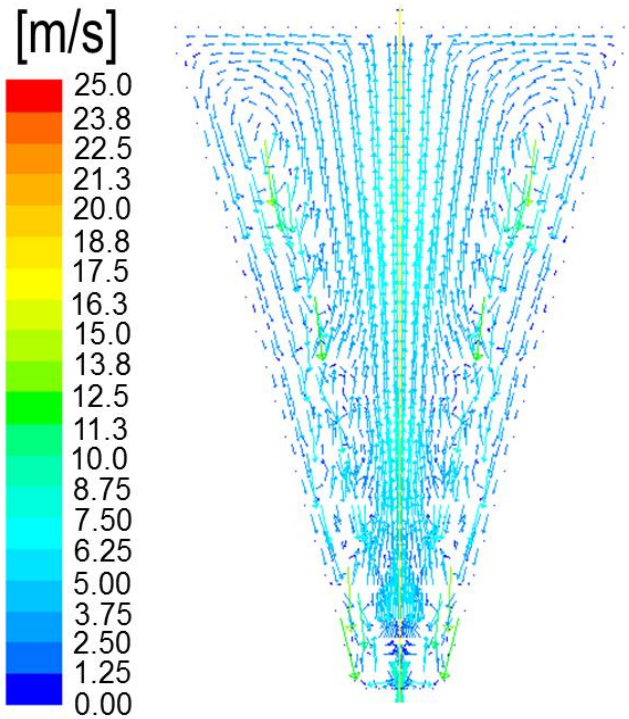

Figure 9: Gas velocity vectors and magnitude [m/s] @ t= 480 mins

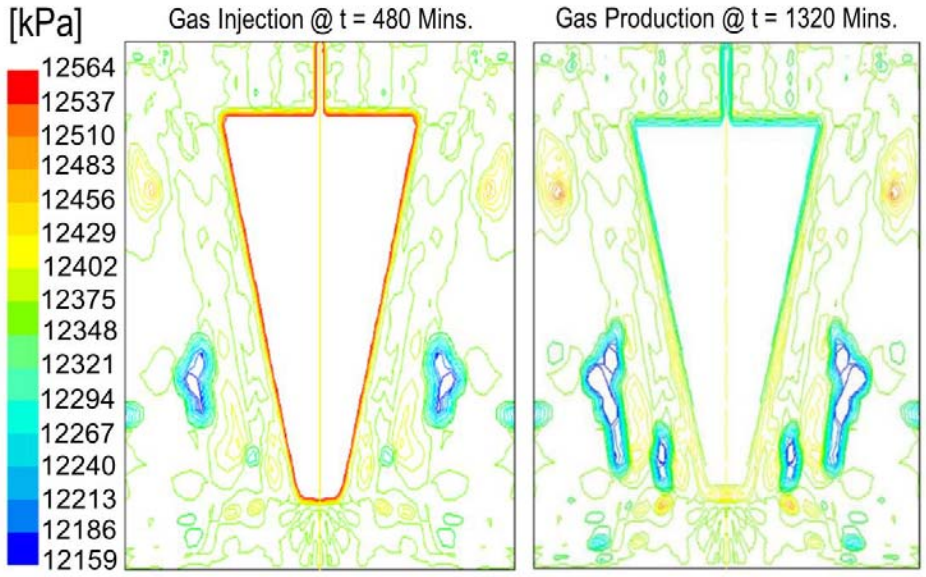

Figure 10: Salt formation gas pressure contours

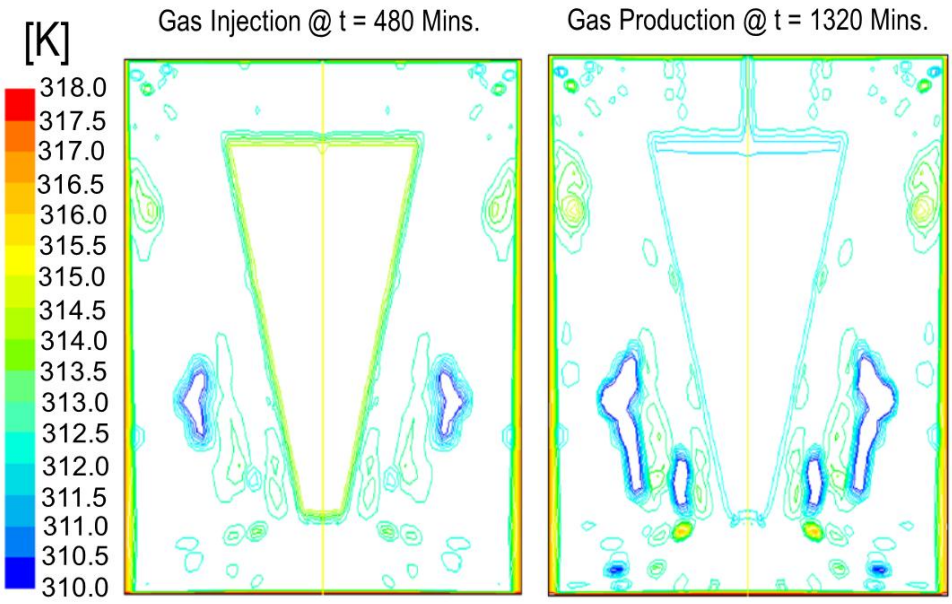

Figure 11: Salt formation gas temperature contours

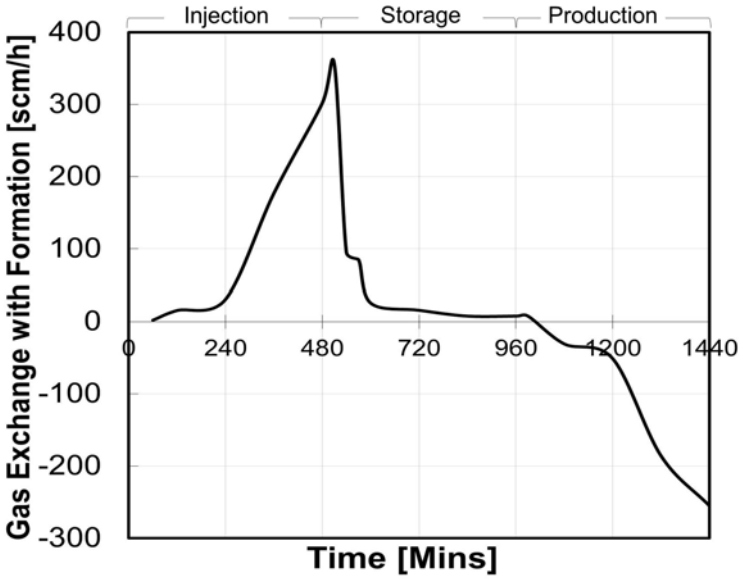

Figure 12: Gas exchange between cavern and salt formation. Positive values indicate gas leak-off, while negative values represent gas leak-in.

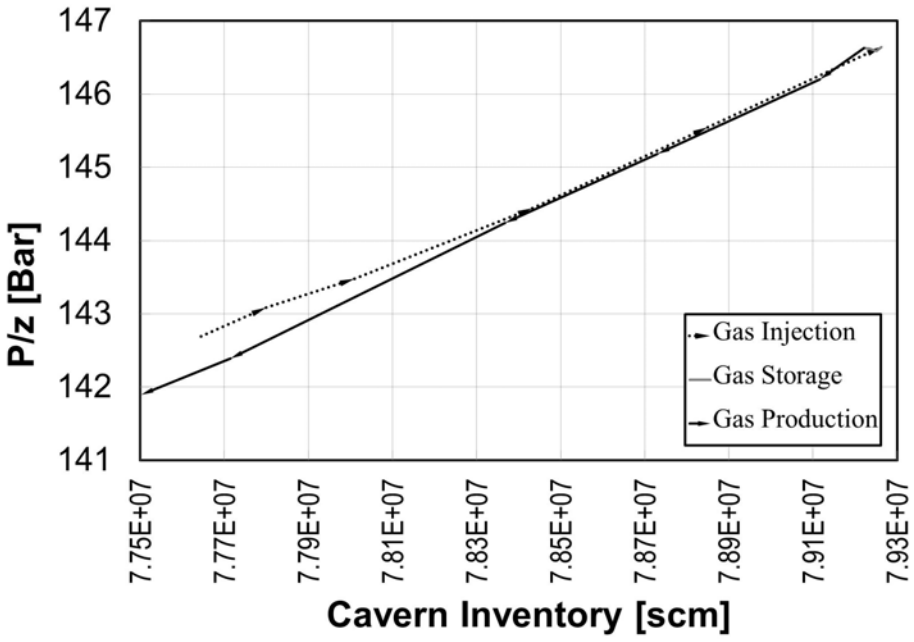

Figure 13: Inventory plots for a 24-hour gas storage operation cycle

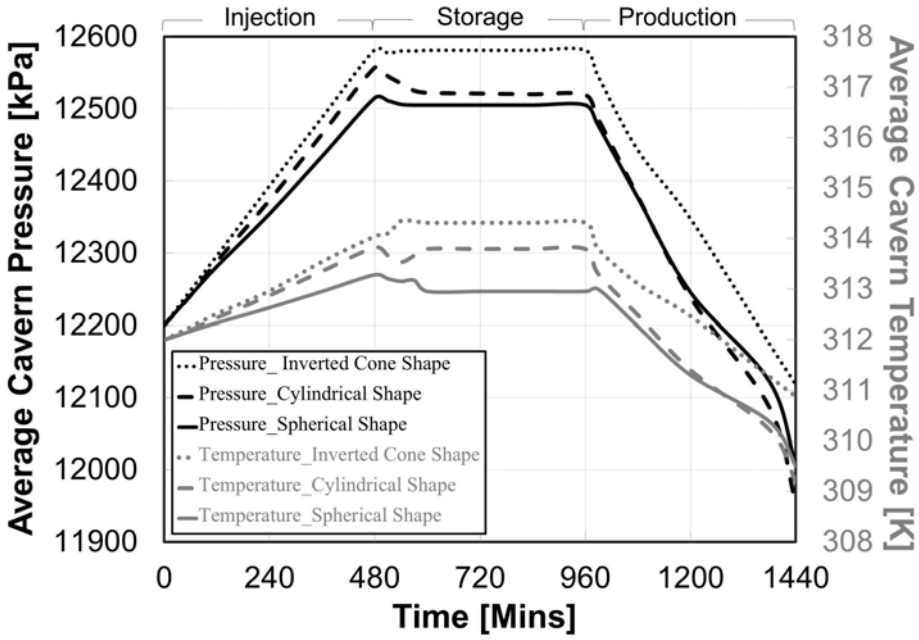

Figure 14: Average cavern pressure and temperature during injection, storage and production for three cavern configurations

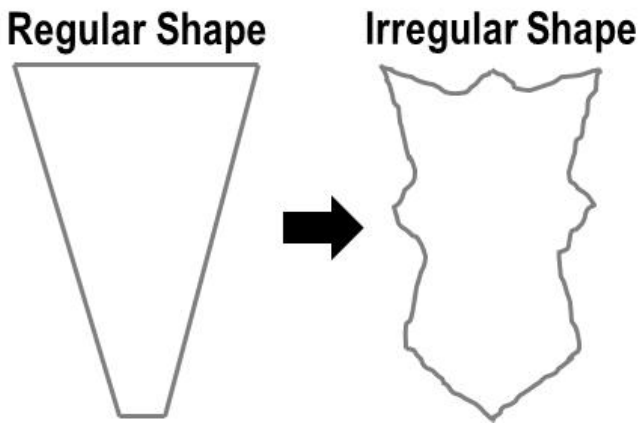

Figure 15: Illustration of regular and irregular cavern shape

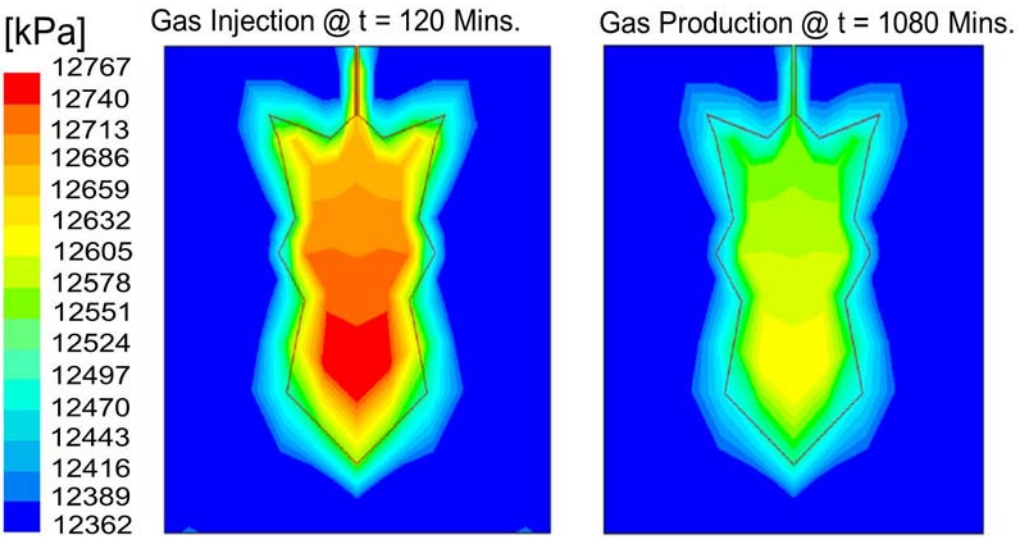

Figure 16: Irregular gas cavern pressure distribution

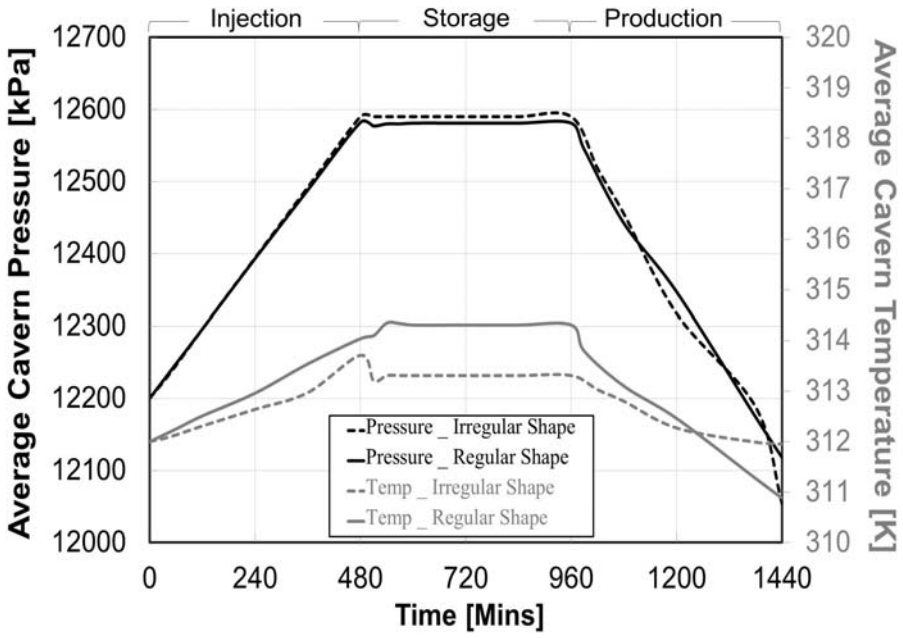

Figure 17: Comparison of average cavern pressure and temperature during injection, storage and production for irregular and regular shapes